Article

The Photoionization Processes of Deep Trap Levels in n-GaN Films Grown by MOVPE Technique on Ammono-GaN Substrates

Piotr Kruszewski [1,*], Konrad Sakowski [1,2], Krzysztof Gościński [3] and Paweł Prystawko [1]

[1] Institute of High Pressure Physics, Polish Academy of Sciences, Sokolowska 29/37, 01-142 Warsaw, Poland; konrad@unipress.waw.pl (K.S.); pprysta@unipress.waw.pl (P.P.)
[2] Institute of Applied Mathematics and Mechanics, University of Warsaw, Banacha 2, 02-097 Warsaw, Poland
[3] Institute of Physics, Polish Academy of Sciences, Al. Lotników 32/46, 02-668 Warsaw, Poland; kgosc@ifpan.edu.pl
* Correspondence: kruszew@unipress.waw.pl

Abstract: In this paper, we present various theoretical models that accurately approximate the spectral density of the optical capture cross-section (σ_e^0) obtained through the analysis of photocapacitance transients using the deep-level optical spectroscopy (DLOS) technique applied to semi-transparent Ni/Au Schottky barrier diodes (SBDs) fabricated on n-GaN films. The theoretical models examined in this study involved a variety of approaches, from the Lucovsky model that assumes no lattice relaxation to more sophisticated models such as the Chantre–Bois and the Pässler models, which consider the electron–phonon coupling phenomenon. By applying theoretical models to the experimentally determined data, we were able to estimate the photoionization (E^0), trap level position (E_T), and Franck–Condon (d_{FC}) energy, respectively. In addition, the results of our analysis confirm that the photoionization processes of deep traps in n-GaN grown by the metal–organic vapor-phase epitaxy technique (MOVPE) are strongly coupled to the lattice. Moreover, it was shown that the Pässler model is preferred for the accurate determination of the individual trap parameters of defects present in n-GaN films grown on an Ammono-GaN substrate. Finally, a new trap level, Ec-1.99 eV with d_{FC} = 0.15, that has not been previously reported in n-GaN films grown by MOVPE was found.

Keywords: GaN; DLOS; deep traps; photoionization; Franck–Condon shift

Citation: Kruszewski, P.; Sakowski, K.; Gościński, K.; Prystawko, P. The Photoionization Processes of Deep Trap Levels in n-GaN Films Grown by MOVPE Technique on Ammono-GaN Substrates. *Appl. Sci.* **2024**, *14*, 8785. https://doi.org/10.3390/app14198785

Received: 29 August 2024
Revised: 25 September 2024
Accepted: 27 September 2024
Published: 29 September 2024

Copyright: © 2024 by the authors. Licensee MDPI, Basel, Switzerland. This article is an open access article distributed under the terms and conditions of the Creative Commons Attribution (CC BY) license (https://creativecommons.org/licenses/by/4.0/).

1. Introduction

It is commonly accepted that due to significant electron–phonon interactions in nitrides, the photoionization processes of deep trap levels in GaN (Eg = 3.4 eV) and $Al_xGa_{1-x}N$ alloys should be strongly coupled to the lattice [1–4]. Experimentally, the electron-phonon coupling phenomenon is manifested i.e. through a much higher optical ionization energy threshold (E^0) required to promote electrons captured on a trap level to the conduction band (C_B) observed in absorption measurements such as SSPC (Steady-State-Photo-Capacitance) [5] and DLOS [6,7] than it would solely result from the position of a trap level in the bandgap. Therefore, the photoionization energies measured in GaN are typically shifted to higher energies by a Franck–Condon factor (d_{FC}), which is related to lattice deformation around a defect that changes its charge state after the photoionization process [8,9].

As previously proposed in numerous papers [8,10], the electron–phonon interaction can be conveniently described in terms of a configuration coordinate diagram (CC) shown schematically in Figure 1. In general, the CC diagram represents the total potential energy of the electronic and lattice vibration subsystems, which are represented by parabolas and horizontal lines within the parabolas, respectively. In this simple model, a defect can be described by a generalized coordinate Q that is proportional to the bond length around

the impurity. Thus, the energy of the system can be expressed by a simple relation where energy is approximately proportional to Q squared ($E \sim Q^2$) as the bonds behave like a harmonically vibrating spring.

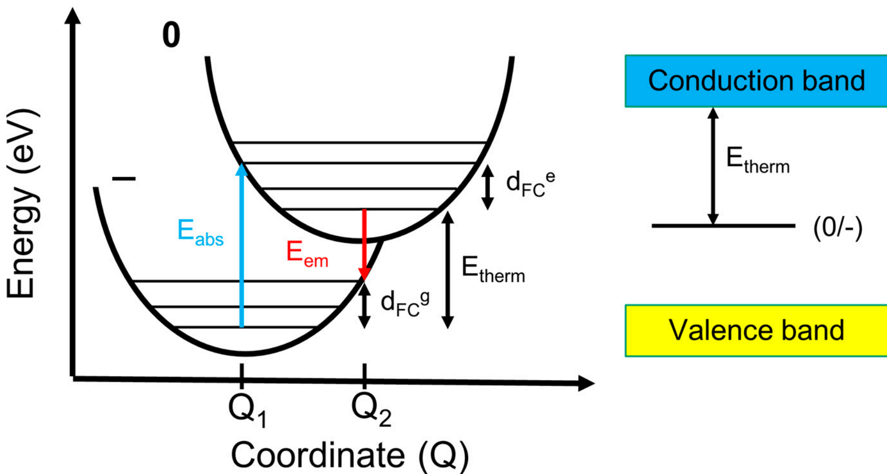

Figure 1. Configuration coordinate diagram describing electron–phonon coupling for an acceptor defect state (0/−). The arrows represent optical transitions as well as specific energies used in CC model.

Furthermore, the CC model assumes that the electron–lattice coupling is a linear function of Q. Therefore, the minima of both parabolas shown in Figure 1 are horizontally displaced and correspond to the generalized coordinates Q_1 and Q_2 in two different defect charge states, respectively.

It is also important to note that in the CC model, optical transitions occur instantly and vertically, whereas thermal transitions are much slower processes that occur laterally through phonon emission or absorption. This depends on the difference between the initial and the final phonon states, represented as horizontal lines in Figure 1. If phonon states are equally distributed in both charge states, the parabolas' minima are vertically shifted by a factor E_{therm}, which is the thermal activation energy commonly measured with a deep-level transient spectroscopy technique (DLTS) [11].

It can be shown that in thermodynamic equilibrium, the total energy of the system with the electron occupying the trap level is minimized for a given Q_1 value (left parabola in Figure 1). However, this situation is remarkably different when a photon is absorbed (E_{abs}) and the electron is promoted to the conduction band. This process is depicted as an optical transition (blue vertical arrow) in Figure 1. In the case of an acceptor trap level (as discussed in this example), this transition results in a change in the charge state from negative to neutral. Since the defect has changed its charge state, the bond lengths are slightly different than in the initial Q_1 state, and the excess energy in the form of phonons ($d_{FC}{}^{e}$) is transferred to the lattice, which results in plastic deformation around the impurity and a new equilibrium state, denoted now as Q_2 (minimum of the right parabola in Figure 1), is obtained.

Similarly, if the electron is recaptured into the trap level, the process is reversed, and the system recovers to its initial Q_1 state through the emission of photons with a characteristic energy (E_{em}), which can be measured by the photoluminescence technique (PL). Again, this process is followed by the reconfiguration of atoms close to the defect and the transfer of energy in the form of phonons ($d_{FC}{}^{g}$) released into the lattice until an equilibrium state is achieved.

If a large number of phonons participate in the photoionization process, the optical capture cross-section of electrons can be approximated by the Huang–Rhys approach [12]. This approach separates both the electron and phonon terms of the optical capture cross-section, and σ_e^0 can be calculated as the product of the electronic part and a Gaussian

function representing the phonon term, which takes into account the broadening effects related to lattice vibrations [13]. This approach has been successfully implemented in the Chantre–Bois [6] and Pässler [7] models, commonly used for modeling the optical capture cross-section in nitrides and other materials. Meanwhile, if the electron–phonon coupling is negligible ($d_{FC} \to 0$), the optical capture cross-section has a purely electronic character and can be approximated with the Lucovsky model [14].

In general, the processes of photoionization of deep trap levels can be described by the spectral dependence of the optical capture cross-section, where the photoionization energy is usually determined by fitting a theoretical model describing the photoionization process to the experimental data. In this procedure, E^0 and d_{FC} are used as fitting parameters. It is evident that E^0, ${d_{FC}}^e$, and $E_T = E_{therm}$ are characteristic and unique parameters that explicitly define any defect level within the bandgap. If these parameters are precisely identified, they can facilitate the accurate and unambiguous recognition of defects. As illustrated in Figure 1, all of the aforementioned parameters are self-dependent and can be expressed by the relation $E_{abs} = E_0 = {d_{FC}}^e + E_T$.

In this study, the optical capture cross-section was determined from the analysis of the photo-capacitance transients, as reported in our recent paper [15]. Accordingly, the Lucovsky [14], Chantre–Bois [6], and Pässler [7] models were fitted to the spectral shape of the optical capture cross-section that was experimentally determined using the formula:

$$\sigma_e^0(h\upsilon) = \frac{e^0}{\phi(h\nu)} = \frac{2N_D}{\phi(h\nu)N_T C}\frac{dC(t)}{dt}\bigg|_{t\to 0} \quad (1)$$

where C is the initial diode capacitance, N_D is the net donor concentration, N_T is the trap level concentration, and C(t) is the photo-capacitance transient, respectively.

Below, we present the results of fitting the theoretical models to our experimental data, followed by a brief discussion of the defect parameters determined from the fitting procedure. Moreover, some variations in E_T and d_{FC} obtained from the Chantre–Bois and the Pässler models are discussed, and a couple of possible reasons for these discrepancies between both models are given.

We would like to emphasize that due to the lack of native GaN substrates essential for obtaining high-quality GaN films, numerous GaN and $Al_xGa_{1-x}N$ layers studied with SSPC and DLOS techniques have commonly been grown on foreign, lattice-mismatched sapphire templates [2–4]. This practice may result in the formation of strained films and high dislocation densities in the overgrown layers, which significantly affect the experimental data and complicate the interpretation of results. In contrast, Ammono-GaN, a native GaN substrate used in this study for an epitaxially deposited n-GaN film, exhibits exceptional structural quality, as validated in various reports [16,17]. More importantly, it has a threading dislocation density (TDD) of approximately 4×10^4 cm^{-2}, which is at least two orders of magnitude lower than that of other native GaN substrates and four orders lower than in GaN films grown on sapphire [18,19]. These superior properties are transferred to overgrown GaN films, which are strain-free when grown on Ammono-GaN. Consequently, this allows for the reliable and unambiguous analysis of experimental results obtained from such samples.

To the best of our knowledge, there have been no studies investigating deep traps using the DLOS technique in terms of electron–lattice coupling effects in n-GaN films grown by MOVPE on Ammono-GaN. This paper aims to fill that gap in the literature. Our approach allows for the precise identification of signatures corresponding to individual trap states, as demonstrated in the following. This study is original and represents a significant advancement in the field.

2. Experimental Details

The samples used in this study were 1.5 µm thick Si-doped n-GaN films grown by the MOVPE technique on a highly conductive Ammono-GaN (n~1×10^{19} cm^{-3}) substrate [16,17]. As the epi structure was grown, the n-GaN sample was cleaved into smaller pieces, and

SBDs on individual chips were fabricated with Ti/Al-based ohmic contacts deposited on the back side of the sample by thermal evaporation with metal thicknesses of 30 and 60 nm, respectively, and sintered at 850 °C, while semi-transparent 10 nm thick Ni Schottky contacts with a diameter of 800 μm were deposited on the n-GaN film using lithography-based techniques. More details on the growth conditions and SBD formation can be found in our other papers in refs. [15,20].

In the SSPC and DLOS measurements, a high-intensity UV-VIS-NIR light source was used to cover the entire spectral range from 1.6 eV to 3.5 eV. The photon flux (ϕ) measured at the sample surface was maintained at a minimum of 5×10^{15} photons·cm^{-2}s^{-1} across the entire spectral range of interest. Due to limitations in accurately determining the absolute light absorption and reflection on the sample surface, the optical capture cross-section data are presented in arbitrary units. The photo-transients were measured at reverse bias, $U_R = -0.5$ V, and the SSPC and DLOS spectra were collected so that the last point of the photo-induced individual transient for each incident photon energy corresponded to the steady-state photo-capacitance signal and the SSPC spectra could be drawn accordingly. In turn, the spectral shape of the optical capture cross-section was determined from the derivative of the initial part of the capacitance transients calculated immediately after the start of illumination (t = 0) for each photon energy using (1). More details on the experimental methodology in the DLOS measurement, as well as the determination of the capture cross-section used in this study, can be found in refs [15,21].

3. Results and Discussion

In Figure 2, we present the AFM (atomic force microscope) topography scan of the n-GaN film deposited on the Ammono-GaN substrate. The GaN surface was atomically flat, characterized by straight atomic steps, with a root-mean-square (RMS) roughness measured for a 3×3 μm^2 square below 0.14 nm. This was significantly lower than the RMS roughness of over 0.4 nm typically reported for GaN films grown by MOVPE on Al_2O_3 substrates [22]. These results clearly demonstrate the superior surface morphology of the GaN layers studied in this paper.

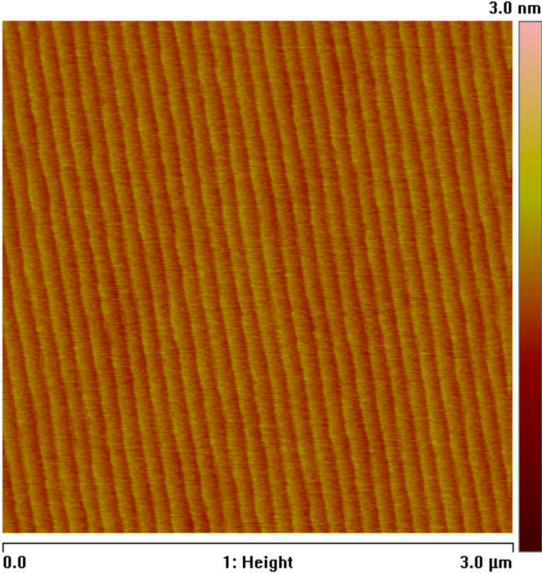

Figure 2. AFM topography of the n-GaN films grown on Ammono-GaN substrate for a square of 3×3 μm^2.

Additionally, the high structural quality of GaN and the $Al_xGa_{1-x}N$ films and crystals grown on Ammono-GaN was previously validated by XRD (X-ray diffraction) measurements as well. These results can be found in our other papers referenced in refs. [23,24].

The n-GaN film investigated in this study was grown on a highly conductive substrate. Therefore, neither the electron concentration nor mobility could be determined

through standard Hall effect measurements typically used for evaluating the electrical transport parameters of semiconducting materials. To address this issue, we employed capacitance–voltage (C-V) measurements at 300 K on processed Ni SBDs to assess the electrical characteristics of the n-GaN film. Our analysis revealed a net donor concentration, $N_D–N_A$, of approximately 2×10^{16} cm^{-3}. A comprehensive examination of the electrical properties of the semitransparent Ni SBDs, using both the C-V and current–voltage (I-V) measurements, has been discussed in detail in our recent publication [15] and, therefore, is not repeated here.

Before characterizing the deep traps using SSPC and DLOS measurements, the Ni/GaN SBDs were investigated with the DLTS technique to identify relatively shallow trap levels. The corresponding DLTS spectrum for the Ni SBDs, recorded at a rate window of 20 s^{-1} with a filling time (t_P) of 1 ms, is shown in Figure 3. Two trap levels were identified at energies of Ec–0.25 eV and Ec–0.59 eV, with concentrations of 2×10^{12} cm^{-3} and 6.7×10^{13} cm^{-3}, respectively. These trap levels are frequently reported in n-GaN films grown by MOVPE [20,25]. Notably, the origin of the deeper trap state at Ec–0.59 eV has been previously identified as being associated with Fe_{Ga} (0/−) [25], which is an acceptor. In contrast, the potential source of the trap level at Ec–0.25 eV has been discussed in detail in reference [20], but its origin remains unknown.

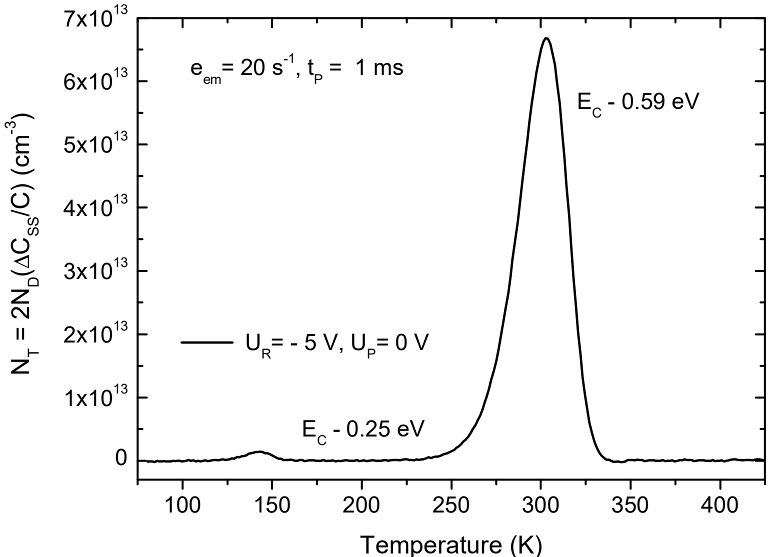

Figure 3. DLTS spectrum for a rate window of 20 s^{-1} measured for Ni SBD for a filling time t_P = 1 ms.

A typical SSPC spectrum for Ni/GaN SBDs measured at T = 293 K is shown in Figure 4, where the Y-axis was recalculated to represent the trap concentration (N_T) using the formula:

$$N_T = 2N_D(\Delta C_{ss}/C) \quad (2)$$

where N_D is the net donor concentration, ΔC_{ss} is the change in the steady-state photocapacitance transient, and C is the capacitance measured with the bias applied to the sample, here, $U_R = -0.5$ V. The capture cross-section data obtained from the DLOS measurements calculated from (1) and plotted as empty squares are presented in the inset of Figure 4. The red solid lines in the inset illustrate the Lucovsky model ($d_{FC} = 0$) fitted to the experimental data points according to the theoretical model given by

$$\sigma_e^0(h\nu) \sim \frac{(h\nu - E_T)^{\frac{3}{2}}}{(h\nu)^3} \quad (3)$$

where E_T represents the trap level position in the bandgap with respect to the conduction band edge, and hν is the photon energy. Accordingly, the E_T values modeled with the Lucovsky approach were found to be E_C–2.05 eV, E_C–2.75 eV, and E_C–3.33 eV, respectively.

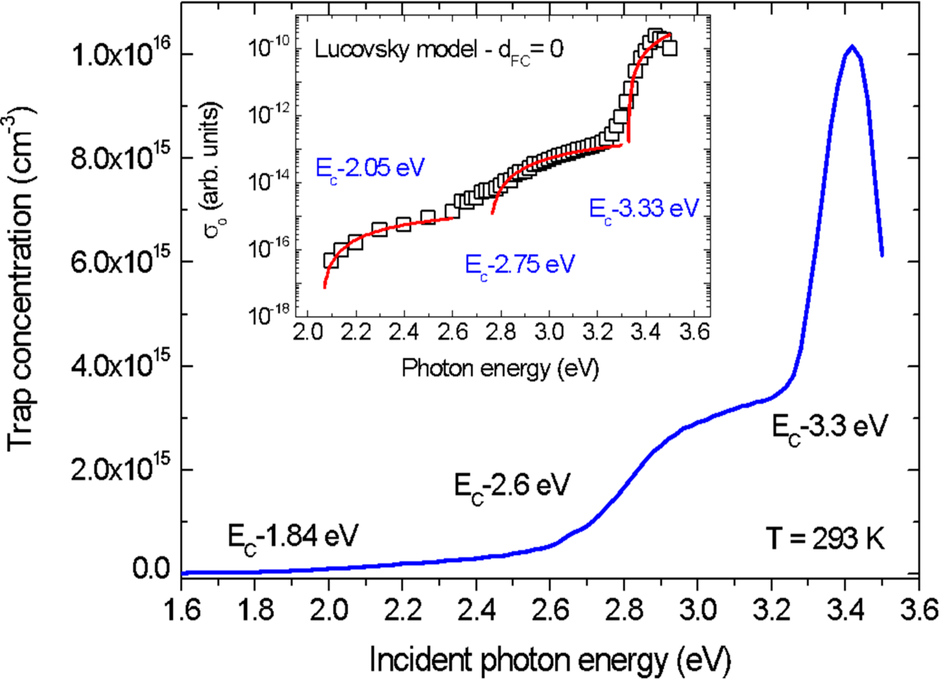

Figure 4. SSPC spectrum for Ni/GaN SBDs measured at T = 293 K with Y-axis recalculated to trap concentration N_T. Inset shows capture cross-section data determined from DLOS measurements using (1) and fitted with Lucovsky model (d_{FC} = 0).

For n-type materials, the positive onsets in the SSPC spectra, as shown in Figure 4, correspond to the trap level positions relative to E_C [5]. However, due to phonon–lattice coupling effects in GaN that are visible as broad steps (or plateaus) in the SSPC spectra, it is difficult to estimate the exact trap level position solely from them. Moreover, since no information about coupling can be deduced from this approach, trap levels' positions derived in this manner can be considered only as vague approximations. Therefore, theoretical models describing photoionization processes have to be used for the accurate determination of deep-level parameters, such as E_T and d_{FC}.

In Figure 5a, the spectral dependencies of the electron photoionization cross-section for three trap levels detected in the Ni/GaN SBDs are shown. Figure 5b–d present the same spectral dependencies as shown in Figure 5a but focus on the individual trap levels only and are displayed over a limited energy range for clarity and visualization purposes. Moreover, the levels positions shown in Figure 5a–d highlighted in the red color correspond to the E_T derived from the Lucovsky model fitting (d_{FC} = 0).

It is clear from Figure 5a–d that the experimental data of the capture cross-section for traps with Ec–2.75 eV and Ec–2.05 eV correspond to a significantly broader range than suggested by a purely electronic excitation model. The unusually large extension of the low-energy tail observed for these traps indicate a strong electron–lattice coupling. Therefore, the lines in Figure 5a–d were fitted to the experimentally determined optical capture cross-sections based on the models proposed by Lucovsky (red), Chantre–Bois (blue), and Pässler (green). The Lucovsky fit in Figure 5a–d was obtained using (3), while the Pässler and Chantre–Bois fits were modeled using the following formulas:

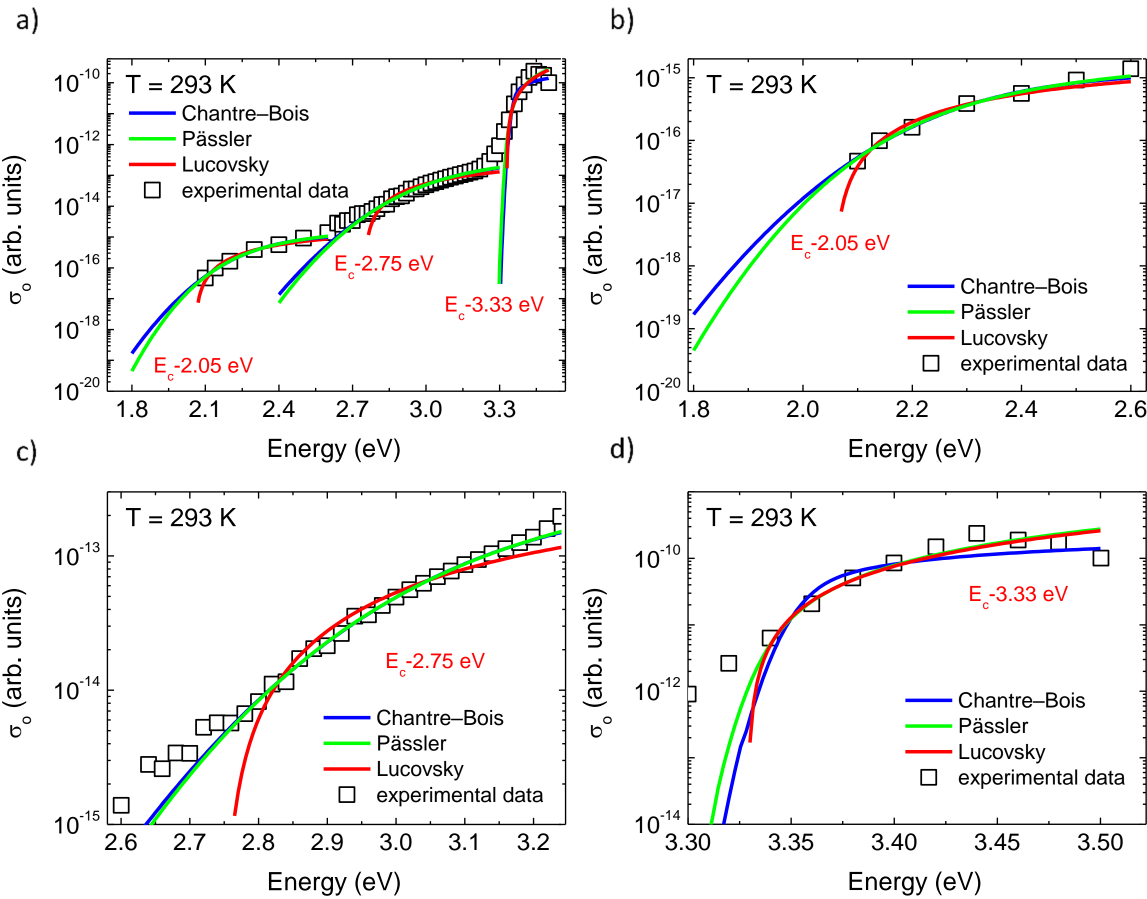

Figure 5. Spectral dependence of electron photoionization cross-section for (**a**) entire spectral range; (**b**) a trap with Ec–2.05 eV; (**c**) for a trap with Ec–2.75 eV; and (**d**) a trap with Ec–3.33 eV, respectively. The red, blue and green solid lines correspond to theoretical models of Lucovsky, Chantre–Bois, and Pässler, respectively.

For the Pässler model,

$$\sigma_e^0(h\upsilon, T) \sim \frac{1}{h\upsilon\sqrt{2\pi d_{FC}\varepsilon\coth(\varepsilon/2k_BT)}} \times \int_0^\infty dE_k \frac{E_k^{3/2}}{\left(E_k + E^0 - d_{FC}\right)^2} \times \exp\left[-\frac{\left(h\upsilon - E^0 - E_k\right)^2}{2d_{FC}\varepsilon\coth\left(\frac{\varepsilon}{2k_BT}\right)}\right] \quad (4)$$

For the Chantre–Bois model,

$$\sigma_e^0(h\upsilon, T) \sim \frac{1}{y\theta^{1/2}} \times \int_1^\infty dx \frac{(x-1)^{1/2}}{\left(x - 1 + E^i/E^0\right)^2} \times \exp\left[-\frac{(y-x)^2}{\theta}\right] \quad (5)$$

where $\theta = \frac{4d_{FC}k_BT}{E^{0^2}}$, $y = \frac{h\upsilon}{E^0}$, and $E_i = \frac{h^2\alpha^2}{2m^*}$, where m^* is the electron effective mass of $0.22\ m_0$, E^0 is the optical ionization energy, and d_{FC} is the Franck–Condon energy shift, and $E^0 = d_{FC} + E_T$. The nonnegative parameter θ corresponds to photon–phonon interactions, which are assumed to be proportional to a normal distribution, with a variance of θ/2. If θ is low, either due to a low temperature or a small Franck–Condon shift, then the phonon contribution is limited, and the distribution is focused on the incident photon energy. Conversely, if θ is large, which implicates both a high temperature and Franck–Condon shift, then the distribution is broad, and the impact of the interaction with phonons becomes significant. Parameter θ in the Chantre–Bois model plays a similar role to the parameter $d_{FC}\varepsilon\coth\left(\frac{\varepsilon}{2k_BT}\right)$ in the Pässler model. However, these models are not equivalent,

especially for a small Franck–Condon shift, as the Pässler model is similar to the Lucovsky model, while the Chantre–Bois model is not (due to the 1/2 power in the numerator of the first term under the integral instead of 3/2). The E_k parameter used in the Pässler model corresponds to the kinetic energy of the excited electron [7]. The α parameter used in the Chantre–Bois model is a fitting parameter that effectively adjusts the mass of the trapped electron, providing a means to fine-tune the model's accuracy.

In Table 1, the parameters of the trap levels extracted from the DLOS data fitted with the three models are summarized. These include the optical ionization energy (E^0), the trap level position (E_T), and the d_{FC} values for all identified trap states. In turn, the individual trap concentrations given in Table 1 were derived from the SSPC data shown in Figure 4.

Table 1. Summary of deep trap state parameters determined from Lucovsky, Chantre–Bois, and Pässler models fitted to σ_e^0 data obtained from DLOS spectra shown in Figure 5a–d.

Model/Trap Concentration	Ec–2.05 eV			Ec–2.75 eV			Ec–3.33 eV		
	E^0 (eV)	E_T (eV)	d_{FC} (eV)	E^0 (eV)	E_T (eV)	d_{FC} (eV)	E^0 (eV)	E_T (eV)	d_{FC} (eV)
Lucovsky	2.05	2.05	0	2.75	2.75	0	3.33	3.33	0
Chantre–Bois	2.28	1.88	0.4	3.07	2.42	0.65	3.35	3.35	0.002
Pässler	2.14	1.99	0.15	2.91	2.61	0.3	3.33	3.33	0.001
Trap concentration (cm^{-3})	3×10^{14}			4×10^{15}			1×10^{16}		

One can notice that the results of the σ_e^0 data fitted with the theoretical models, illustrated in Figure 5a–d, may lead to a few general remarks: (1) the Lucovsky model fits the experimental data quite well; however, the trap level positions (E_T) determined from this approach appear to be consistently underestimated in comparison with the Chantre–Bois or Pässler models for trap levels that are strongly coupled to the lattice, i.e., where d_{FC} = 0.15–0.4 and 0.3–0.65 for the Ec–2.05 eV or Ec–2.75 eV trap levels, respectively; (2) in turn, the Lucovsky model applied to the trap level located relatively close to the valence band edge (Ec–3.33 eV) gives almost the same E_T values as the two other models; and (3) significant discrepancies in the defect parameters determined from the Chantre–Bois and Pässler models are observed for states with Ec–2.05 eV and Ec–2.75 eV. The latter occurs despite the fact that both approaches have been developed for modeling trap levels that are strongly coupled with the lattice and, in principle, should give consistent results. Some possible explanations for this discrepancy are proposed below.

In general, our observations on the σ_e^0 data fitted with the Lucovsky model align with the model basis, where the potential of a deep trap center is of the ion core type or can be approximated as a delta function, neglecting any long-range Coulomb effects. This model is particularly relevant for hydrogenic-type defect levels, which are generally shallow and located near band edges. When a defect's wavefunction is delocalized, the electron density at the defect remains low, resulting in minimal influence on the local rearrangements of surrounding atoms, as observed for a trap with Ec–3.33 eV that is located just 70 meV above the valence band edge (V_B). Therefore, it is entirely reasonable to classify this trap level as shallow. Consequently, the wavefunctions of midgap states are strongly localized, and the Lucovsky model is not applicable in this case. However, the E_T determined from this model can still be used as a rough approximation. Furthermore, since the Lucovsky model assumes a purely electronic character for the ionization process, the dependence of the σ_e^0 spectrum on temperature should remain unaffected. This is a distinctive feature of the Lucovsky model and can be easily verified to provide unambiguous proof of whether the trap level can be described with this model or not. Unfortunately, we could only carry out DLOS measurements at 293 K.

In order to explain the discrepancies in the deep trap parameters obtained from the Chantre–Bois and Pässler models, one should reconsider how electron–phonon coupling effects are implemented in both models. In the Pässler model, to quantify the lattice–phonon interaction, the concept of an effective phonon energy, $\varepsilon = \hbar\omega$, was proposed [7]. Therefore,

a magnitude of ε should be precisely determined and then used in the data fitting. In GaN, the phonon energy spectrum is generally known; however, it is rather broad and consists of low- and high-energy components, from 0 to 90 meV, as previously reported [26,27]. If we assume that both components contribute equally, a good approximation could be ε ~ 45–50 meV, as used by Pässler in his original work [7]. However, it is highly recommended to check the calculations with other ε-values to ensure that this parameter has been correctly chosen. In our calculations, the Pässler model with ε = 70 meV provided the best agreement between the theory and the data and, thus, was used in the data fitting presented in Figure 5a–d.

In turn, the Chantre–Bois model applied here for comparison employs a different approach, where the local effective mass of the electron trapped at the defect level is an adjustable parameter denoted as α^{-1}. This parameter describes the localization of the electron wavefunction at the trap level and, therefore, its interaction with the lattice as well. In this study, α^{-1} was individually determined for each trap state and estimated to be 1.67×10^{-3} Å, 5.65×10^{-3} Å, and 1.5 Å for traps with Ec–2.05 eV, Ec–2.75 eV, and Ec–3.33 eV, respectively. Since $\alpha^{-1} \sim 1/\sqrt{m}$, smaller values correspond to a higher effective electron mass and, thus, enhanced localization of the trapped electron wavefunction, as expected for deep trap states [6]. The only α^{-1} value reported so far in the literature is for the E2 trap in n-GaN (Ec–0.56 eV), which is relatively shallow in comparison with midgap states, and was estimated to be 3.3 Å [21]. This result is comparable to α^{-1} = 1.5 Å for a trap with Ec–3.33 eV found in this study. In contrast, the midgap states exhibited significantly lower values of α^{-1}, suggesting a strong coupling to the lattice, as previously reported in other experiments [1–4].

Furthermore, an important distinction between the models is their applicability to the data measured at different temperatures. As indicated in Equation (5), the exponential component of the Chantre–Bois model approaches zero at low temperatures, resulting in $\sigma = 0$. Consequently, this model should be applied to the experimental data carried out at high temperatures. However, as was suggested by Pässler [28], due to a relatively high effective phonon energy, ε ~ 80 meV, the Chantre–Bois model in SiC could be efficient at temperatures above 1000 K, which is beyond the practical temperature range in most experiments. Since the effective phonon energy in GaN is comparable to SiC (ε_{GaN}~ 50–60 meV), it is expected that similar restrictions regarding the temperature limit of the model application should be considered for GaN as well.

In turn, the Pässler model, presented in a more generalized form, as given in (4), has no limitations in terms of temperature and can be effectively applied across low- and high-temperature ranges. Consequently, the experimental data fitting with the Pässler model is expected to provide more precise trap parameters than that determined from the Chantre–Bois model.

Finally, the d_{FC} and E_T obtained in this study from the Pässler model for a trap with Ec–2.75 eV (E_T = 2.61 eV and d_{FC} = 0.3 eV, given in Table 1) are consistent with previously published reports where trap levels of E_T = 2.6 eV and d_{FC} = 0.4 eV were found using the Pässler model [28,29], and this trap level was assigned to carbon-related (C_i or C_N) defects [29]. Since both E_T and d_{FC} reported in refs. [29,30] are in good agreement with the results found in this study, we suggest that both trap states have the same origin.

Unfortunately, the trap level with Ec–2.05 eV has never been reported before so a detailed analysis of this trap level could not be carried out. Therefore, the origin of this particular trap state level is still unknown.

4. Conclusions

The spectral density of the optical capture cross-section for deep trap states in semi-transparent Ni/Au Schottky diodes fabricated on n-GaN films grown by the MOVPE technique on an Ammono-GaN substrate was presented. A variety of approaches were employed, including the Lucovsky model, which assumes no lattice relaxation, as well as models that consider the electron–phonon coupling phenomenon, such as the Chantre–Bois

and the Pässler models. These models were used to estimate the photoionization energy (E^0), trap level position (E_T), and Franck–Condon energy (d_{FC}), respectively. The results of our analysis confirm that most of the photoionization processes of deep traps in n-GaN are strongly coupled to the lattice and, thus, must be analyzed with the models that consider electron–phonon coupling effects. Moreover, we found a new trap level, Ec-1.99 eV with d_{FC} = 0.15, that has not been previously reported in n-GaN films grown by the MOVPE technique. Finally, we approved that the Pässler model originally developed for deep trap analysis in SiC and GaN/AlGaN structures is preferred for the accurate determination of the individual trap parameters of defects present in n-GaN films.

Author Contributions: P.K.: conceptualization (lead); methodology (lead); investigation (lead); data curation (lead); formal analysis (lead); funding acquisition (lead); supervision (lead); visualization (equal); writing—original draft (lead). K.S.: software (lead); validation (equal); visualization (equal); writing—original draft (supporting); formal analysis (supporting). K.G.: formal analysis (supporting); software (supporting). P.P.: resources (lead); investigation (supporting). All authors have read and agreed to the published version of the manuscript.

Funding: This work was financially supported by the National Science Centre, Poland, through project number 2020/37/B/ST5/02593.

Data Availability Statement: The data that support the findings of this study are available from the corresponding author upon reasonable request.

Conflicts of Interest: The authors declare no conflicts of interest.

References

1. Reshchikov, M.A.; Shahedipour, F.; Korotkov, R.Y.; Ulmer, M.P.; Wessels, B.W. Deep acceptors in undoped GaN. *Phys. B Condens. Matter.* **1999**, *273–274*, 105–108. [CrossRef]
2. Armstrong, A.; Poblenz, C.; Green, D.S.; Mishra, U.K.; Speck, J.S.; Ringel, S.A. Impact of substrate temperature on the incorporation of carbon-related defects and mechanism for semi-insulating behavior in grown by molecular beam epitaxy. *Appl. Phys. Lett.* **2006**, *88*, 082114. [CrossRef]
3. Arehart, A.R.; Corrion, A.; Poblenz, C.; Speck, J.S.; Mishra, U.K.; Ringel, S.A. Deep level optical and thermal spectroscopy of traps in n-GaN grown by ammonia molecular beam Epitaxy. *Appl. Phys. Lett.* **2008**, *93*, 112101. [CrossRef]
4. Zhang, Z.; Arehart, A.R.; Kyle, E.C.H.; Chen, J.; Zhang, E.X.; Fleetwood, D.M.; Schrimpf, R.D.; Speck, J.S.; Ringel, S.A. Proton irradiation effects on deep level states in Mg-doped p-type GaN grown by ammonia-based molecular beam epitaxy. *Appl. Phys. Lett.* **2015**, *106*, 022104. [CrossRef]
5. Blood, P.; Orton, J.W. *The Electrical Characterization of Semiconductors: Majority Carriers and Electron States*; Academic Press: San Diego, CA, USA, 1992.
6. Chantre, A.; Vincent, G.; Bois, D. Deep-level optical spectroscopy in GaAs. *Phys. Rev. B* **1981**, *23*, 5335. [CrossRef]
7. Pässler, R. Photoionization cross-section analysis for a deep trap contributing to current collapse in GaN field-effect transistors. *J. Appl. Phys.* **2004**, *96*, 715–722. [CrossRef]
8. Markham, J.J. Interaction of Normal Modes with Electron Traps. *Rev. Mod. Phys.* **1959**, *31*, 956. [CrossRef]
9. Henry, C.H.; Lang, D.V. Nonradiative capture and recombination by multiphonon emission in GaAs and GaP. *Phys. Rev. B* **1977**, *15*, 989–1016. [CrossRef]
10. Alkauskas, A.; McCluskey, M.D.; Van de Walle, C.G. Tutorial: Defects in semiconductors—Combining experiment and theory. *J. Appl. Phys.* **2016**, *119*, 181101. [CrossRef]
11. Lang, D.V. Deep-level transient spectroscopy: A new method to characterize traps in semiconductors. *J. Appl. Phys.* **1974**, *45*, 3023–3032. [CrossRef]
12. Huang, K.; Rhys, A. Theory of light absorption and non-radiative transitions in F-centres. *Proc. Rev. Soc. A* **1950**, *204*, 406. [CrossRef]
13. Mooney, P.M.; Northrop, G.A.; Morgan, T.N.; Grimmeiss, H.G. Evidence for large lattice relaxation at the DX center in Si-doped AlxGa1−xAs. *Phys. Rev. B* **1988**, *37*, 8298. [CrossRef] [PubMed]
14. Lucovsky, G. On the photoionization of deep impurity centers in semiconductors. *Solid State Commun.* **1965**, *3*, 299. [CrossRef]
15. Kruszewski, P.; Sai, P.; Krajewska, A.; Sakowski, K.; Ivonyak, Y.; Jakiela, R.; Plesiewicz, J.; Prystawko, P. Graphene Schottky barrier diode acting as a semi-transparent contact to n-GaN. *AIP Adv.* **2024**, *14*, 075312. [CrossRef]
16. Dwilinski, R.; Doradzinski, R.; Garczynski, J.; Sierzputowski, L.P.; Puchalski, A.; Kanbara, Y.; Yagi, K.; Minakuchi, H.; Hayashi, H. Excellent crystallinity of truly bulk ammonothermal GaN. *J. Cryst. Growth* **2008**, *310*, 3911–3916. [CrossRef]
17. Zajac, M.; Kucharski, R.; Grabianska, K.; Gwardys-Bak, A.; Puchalski, A.; Wasik, D.; Litwin-Staszewska, E.; Piotrzkowski, R.; Domagala, J.Z.; Bockowski, M. Basic ammonothermal growth of Gallium Nitride—State of the art, challenges, perspectives. *Prog. Cryst. Growth Charact. Mater.* **2018**, *64*, 63–74. [CrossRef]

18. Grabianska, K.; Jaroszynski, P.; Sidor, A.; Bockowski, M.; Iwinska, M. GaN Single Crystalline Substrates by Ammonothermal and HVPE Methods for Electronic Devices. *Electronics* **2020**, *9*, 1342. [CrossRef]
19. Lang, T.; Odnoblyudov, M.; Bougrov, V.; Suihkonen, S.; Sopanen, M.; Lipsanen, H. Morphology optimization of MOCVD-grown GaN nucleation layers by the multistep technique. *J. Cryst. Growth* **2006**, *292*, 26–32. [CrossRef]
20. Kruszewski, P.; Kaminski, P.; Kozlowski, R.; Zelazko, J.; Czernecki, R.; Leszczynski, M.; Turos, A. Laplace DLTS studies of the 0.25 eV electron trap properties in n-GaN. *Semicond. Sci. Technol.* **2021**, *36*, 035014. [CrossRef]
21. Hacke, P.; Ramvall, P.; Tanaka, S.; Aoyagi, Y.; Kuramata, A.; Horino, K.; Munekata, H. Optical characterization of the "E2" deep level in GaN. *Appl. Phys. Lett.* **1999**, *74*, 543. [CrossRef]
22. Kyle, E.C.H.; Kaun, S.W.; Burke, P.G.; Wu, F.; Wu, Y.R.; Speck, J.S. High-electron-mobility GaN grown on free-standin GaN templates by ammonia-based molecular beam epitaxy. *J. Appl. Phys.* **2014**, *115*, 193702. [CrossRef]
23. Kruszewski, P.; Prystawko, P.; Kasalynas, I.; Nowakowska-Siwinska, A.; Krysko, M.; Plesiewicz, J.; Smalc-Koziorowska, J.; Dwilinski, R.; Zajac, M.; Kucharski, R.; et al. AlGaN/GaN HEMT structures on ammono bulk GaN substrate. *Semicond. Sci. Technol.* **2014**, *29*, 075004. [CrossRef]
24. Iwinska, M.; Takekawa, N.; Ivanov, V.Y.; Amilusik, M.; Kruszewski, P.; Piotrzkowski, R.; Litwin-Staszewska, E.; Lucznik, B.; Fijalkowski, M.; Sochacki, T.; et al. Crystal growth of HVPE-GaN doped with germanium. *J. Cryst. Growth* **2017**, *480*, 102–107. [CrossRef]
25. Horita, M.; Narita, T.; Kachi, T.; Suda, J. Identification of origin of EC–0.6 eV electron trap level by correlation with iron concentration in n-type GaN grown on GaN freestanding substrate by metalorganic vapor phase epitaxy. *Appl. Phys. Express* **2020**, *13*, 071007. [CrossRef]
26. Nipko, J.C.; Loong, C.-K.; Balkas, C.M.; Davis, R.F. Phonon density of states of bulk gallium nitride. *Appl. Phys. Lett.* **1998**, *73*, 34–36. [CrossRef]
27. Bungaro, C.; Rapcewicz, K.; Bernholc, J. Ab initio phonon dispersions of wurtzite AlN, GaN, and InN. *Phys. Rev. B* **2000**, *61*, 6720. [CrossRef]
28. Pässler, R. Alternative electronic parts for multiphonon-broadened photoionization cross sections of deep levels in SiC. *J. Appl. Phys.* **2005**, *97*, 113533. [CrossRef]
29. Armstrong, A.; Arehart, A.R.; Green, D.; Mishra, U.K.; Speck, J.S.; Ringel, S.A. Impact of deep levels on the electrical conductivity and luminescence of gallium nitride co-doped with carbon and silicon. *J. Appl. Phys.* **2005**, *98*, 053704. [CrossRef]
30. Li, W.; Zhang, Y.; Chen, Z.; Zhao, H.; Ringel, S.A.; Arehart, A.R. Trap characterization of high-growth-rate laser-assisted MOCVD GaN. *Appl. Phys. Lett.* **2023**, *123*, 112101. [CrossRef]

Disclaimer/Publisher's Note: The statements, opinions and data contained in all publications are solely those of the individual author(s) and contributor(s) and not of MDPI and/or the editor(s). MDPI and/or the editor(s) disclaim responsibility for any injury to people or property resulting from any ideas, methods, instructions or products referred to in the content.